Journal of Solid State Chemistry 181 (2008) 2217–2226

Contents lists available at ScienceDirect

Journal of Solid State Chemistry

journal homepage: www.elsevier.com/locate/jssc

Structural chemistry and magnetic properties of $Pr_{3-x}Sr_{1+x}CrNiO_8$

Siân E. Dutton [a], Mona Bahout [b,*], Peter D. Battle [a,*], Florent Tonus [b], Valérie Demange [c]

[a] Inorganic Chemistry Laboratory, Oxford University, South Parks Road, Oxford OX1 3QR, UK
[b] Laboratoire des Sciences Chimiques de Rennes, Université de Rennes 1, UMR CNRS 6226, 263 Avenue du Général Leclerc, 35042 Rennes Cedex, France
[c] Laboratoire de Science et Génie des Surfaces, UMR 7570 CNRS, Institut Jean Lamour, FR2797/CNRS, Nancy-Université, Ecole des Mines de Nancy, Parc de Saurupt, CS14234, 54042 Nancy Cedex, France

ARTICLE INFO

Article history:
Received 2 April 2008
Received in revised form
9 May 2008
Accepted 13 May 2008
Available online 18 May 2008

Keywords:
Ruddlesden–Popper
K_2NiF_4 structure
Magnetism
Spin glass

ABSTRACT

Polycrystalline samples of the $n=1$ Ruddlesden–Popper system $Pr_{3-x}Sr_{1+x}CrNiO_8$ have been synthesized over the composition range $0.0<x\leqslant 1.0$ either by the ceramic method or from solution. They have been characterized by an appropriate combination of diffraction methods (X-ray, neutron and electron) and magnetometry (d.c. and a.c.). All compositions having $x>0.1$ adopt the tetragonal space group $I4/mmm$; $Pr_{2.9}Sr_{1.1}CrNiO_8$ adopts the orthorhombic space group $Fmmm$. There is no evidence of Cr/Ni cation ordering in any composition. A maximum in the zero-field cooled magnetic susceptibility is observed at a temperature T_f that decreases with increasing Sr content; $52\leqslant T_f\,(K)\leqslant 13$. The frequency dependence of T_f observed in a.c. susceptibility measurements, together with the analysis of neutron diffraction data, suggests that the atomic magnetic moments in these compositions adopt a spin-glass-like state below T_f.

1. Introduction

Although there are some exceptions [1], the majority of mixed-metal oxides that contain just a single cation species with a partially filled 3*d* shell are electrical insulators that adopt an antiferromagnetic or ferrimagnetic ground state on cooling to low temperatures; ferromagnetism is rare [2,3] other than in mixed-valence compounds, where it often coincides with the occurrence of metallic conductivity [4]. The Goodenough–Kanamori [5] rules predict that if two cation species, *B* and *B*′, with appropriate electron configurations (for example d^3 and d^5 or d^5 and d^8) are present in an insulating oxide, then the superexchange interaction between them can be ferromagnetic, provided that the *B*–O–*B*′ bond angle is close to 180°. However, it is likely that *B*–O–*B* and *B*′–O–*B*′ superexchange interactions will be antiferromagnetic, and they will therefore compete with the *B*–O–*B*′ interactions. In order for the pair-wise ferromagnetic coupling to translate into long-range, bulk ferromagnetism the *B* and *B*′ cations must be distributed through the crystal structure in an ordered manner so as to minimize the effect of the competitive antiferromagnetic interactions. In the absence of such cation ordering, spin-glass behaviour is likely to result. Many attempts have been made to produce new ferromagnets by synthesizing cation-ordered perovskites. The undistorted cubic form of this structure provides the linear superexchange pathways discussed above. However, perovskites often distort to a lower symmetry [6], reducing the *B*–O–*B*′ bond angle to ~160° and hence weakening the ferromagnetic component of the intercation interaction. Furthermore, it is difficult to find two magnetic *d*-block cations with a difference in size or charge that is large enough to cause them to adopt an ordered distribution over the six-coordinate sites of the perovskite structure [7]. An alternative strategy is to try to induce ferromagnetism in the perovskite-related Ruddlesden–Popper (RP) oxides $A_{n+1}B_{0.5}B'_{0.5}O_{3n+1}$. In this paper we deal with the $n=1$ member of this series, often referred to as the K_2NiF_4 structure (Fig. 1). The ideal form of this layered structure has tetragonal symmetry and retains the linear *B*–O–*B*′ linkages found in the undistorted perovskite structure ($n=\infty$). The rigidity of the *A*O layers that separate the perovskite-like BO_2 sheets renders the $n=1$ structure less prone to distortions and it therefore offers more scope for preserving the ferromagnetic nature of the interactions between different cations. However, the issue of cation ordering remains to be addressed. We have previously shown that cation ordering can occur in either two or three dimensions in this structure type [8]. More specifically, in La_4LiMnO_8 the Li^+ and Mn^{3+} cations order within the layers of octahedra that lie perpendicular to [001] but there is no long-range cation ordering between successive layers. In $La_2Sr_2LiRuO_8$ the same pattern of ordering is observed within the layers, but in this case [9] the ordering is also periodic along [001].

* Corresponding authors.
Fax: +33 223 236 799 (M. Bahout), fax: +44 1865 272690 (P.D. Battle).
E-mail addresses: Mona.Bahout@univ-rennes1.fr (M. Bahout), Peter.Battle@chem.ox.ac.uk (P.D. Battle).

0022-4596/$ - see front matter © 2008 Elsevier Inc. All rights reserved.
doi:10.1016/j.jssc.2008.05.017

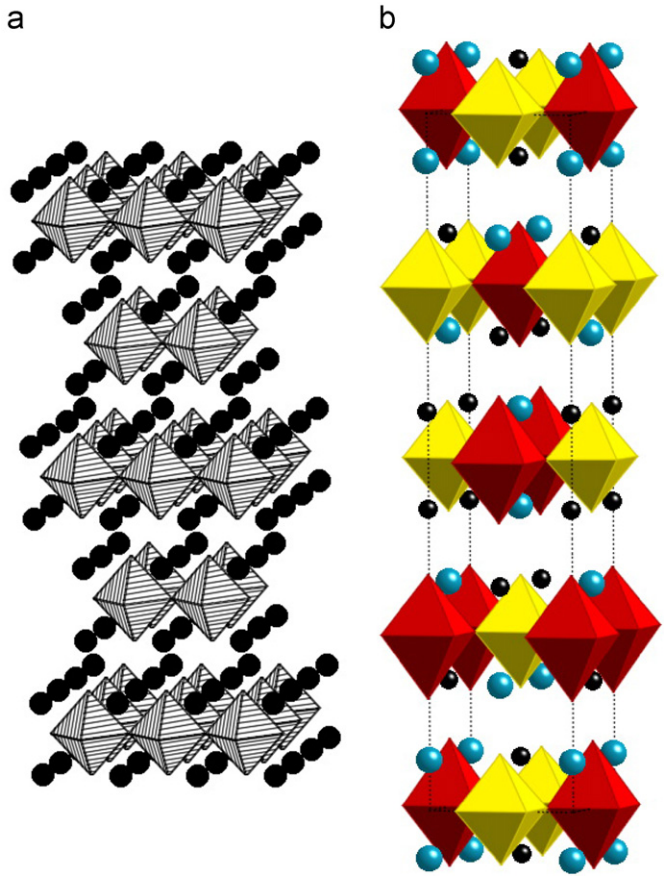

Fig. 1. (a) The $n = 1$ Ruddlesden–Popper structure of A_2BO_4; black circles represent *A*-site cations, octahedra represent BO_6 groups and (b) a representation of the Li/Ru and Sr/La cation ordering observed in $La_2Sr_2LiRuO_8$.

Furthermore, there is a concomitant ordering of the La^{3+} and Sr^{2+} cations over the inter-layer cation sites. This compound was the first $n = 1$ RP phase in which ordering over both sets of cation sites was observed, and the result remains unique. Attempts to reproduce the effect by replacing La^{3+} with other lanthanide cations were unsuccessful, thus demonstrating the sensitivity of the structure to the chemical composition.

In this paper we describe our attempts to prepare new magnetic materials by synthesizing compositions in the system $Pr_{3-x}Sr_{1+x}CrNiO_8$ ($0 \leqslant x \leqslant 1$). Assuming the presence of Pr^{3+}, $Pr_3SrCrNiO_8$ was expected to contain Ni^{2+}:d^8 and Cr^{3+}:d^3, a combination for which both the π and σ superexchange interactions are predicted to lead to ferromagnetic coupling. The introduction of Sr should result in the oxidation of either Pr^{3+} to Pr^{4+} or Ni^{2+} to low-spin Ni^{3+}; neither of these oxidations would eliminate the ferromagnetic coupling within an ordered cation array. The charge difference between the two *B*-site cations is obviously small, but we hoped that their size difference might be large enough to induce the ordering necessary for the establishment of a ferromagnetic state. If the cation ordering occurred only in two dimensions, thus creating ferromagnetic *xy* sheets, then the application of only a small applied field might be expected to align the magnetic moments associated with the individual sheets to create a large net magnetization. We describe below our attempts to synthesize this series of compounds, and the subsequent characterization of our reaction products by magnetometry and diffraction techniques. Our results are compared with those obtained on related RP and perovskite compositions.

2. Experimental

2.1. Synthesis

Attempts were made to prepare samples of $Pr_{3-x}Sr_{1+x}CrNiO_8$ in the composition range $0.0 \leqslant x \leqslant 1.0$ using a standard ceramic synthesis route. Stoichiometric mixtures of starting materials (Pr_6O_{11} (Alfa Aesar, 99.996%), $SrCO_3$ (Alfa Aesar, 99.994%), NiO (Alfa Aesar, 99.998%), Cr_2O_3 (Johnson Matthey, Grade 1)) were intimately ground and fired firstly as a powder at 1000 °C under flowing argon (BOC) for 12 h and then, after regrinding, in pellet form at 1250 °C for 48 h, also under flowing argon. To prevent any loss of reactants the pellets were completely surrounded by a powder 'blanket' of the same composition, thus avoiding direct contact with the alumina crucible and argon atmosphere. Samples were cooled under flowing argon at a rate of 2 °C min^{-1} to 500 °C at which temperature the furnace was switched off and allowed to cool radiatively to room temperature. This regrinding and firing sequence was repeated until a pure product was obtained, as judged by X-ray powder diffraction.

Attempts were also made to prepare $Pr_{3-x}Sr_{1+x}CrNiO_8$ samples in the composition range $0.0 \leqslant x \leqslant 1.0$ using a solution route. Stoichiometric amounts of Pr_6O_{11} (Acros Organics, 99.9%), $Sr(CH_3CO_2)_2 \cdot xH_2O$ (Aldrich, 99.995%), $Cr_3(CH_3CO_2)_7(OH)_2$ (Aldrich) and $Ni(CH_3CO_2)_2 \cdot 4H_2O$ (Aldrich, 99.998%) were dissolved in water acidified with the minimum quantity of 6 M nitric acid necessary to ensure the dissolution of the Pr_6O_{11} at 100 °C. The solution was then heated to dryness with constant stirring. The solid obtained was decomposed by further heating in air at 550 °C for ~24 h and then, after grinding, in pellets at 1200–1300 °C for 2–4 days, under flowing argon. As described above, the pellets were enveloped in powder of the same nominal composition. Samples were cooled under flowing argon at a rate of 2 °C min^{-1} to 550 °C at which point the furnace was switched off and allowed to cool to room temperature. The regrinding and firing sequence was repeated until a pure product was obtained, the progress of the reaction being monitored by X-ray powder diffraction.

2.2. Characterization

High-resolution X-ray powder diffraction patterns for use in quantitative analysis were collected on a Philips X'Pert diffractometer operating with Cu $K\alpha_1$ radiation or a Bruker D5000 operating with Cu $K\alpha$ radiation. Data were collected over the angular range $5 \leqslant 2\theta\,(\text{deg}) \leqslant 125$ with a step size of $\Delta 2\theta = 0.0084^\circ$ (X'Pert) or 0.02° (D5000). Rietveld [10] refinement of the structures was carried out using either the GSAS [11] or FULLPROF [12] program suites. Backgrounds were fitted using a Chebyshev polynomial of the first kind and the peak shape was modelled using a pseudo-Voigt function.

Neutron powder diffraction data were collected on selected samples on D2b at the Institute Laue Langevin, Grenoble, France, a high-flux, high-resolution instrument operating at $\lambda = 1.59147$ Å. Data were collected over the angular range $5 \leqslant 2\theta\,(\text{deg}) \leqslant 160$ with a step size of $\Delta 2\theta = 0.05^\circ$ at a temperature of 5 K. Samples were contained within vanadium cans which were mounted in a Displex refrigerator. Rietveld refinements of the structures were carried out using the FULLPROF suite of programs. Backgrounds were estimated manually and then refined using the software. Peak shapes were modelled using a pseudo-Voigt function employing three peak asymmetry parameters refined below $2\theta = 54^\circ$.

The composition $x = 0.5$ was prepared by both synthetic routes. In order to compare the two samples at the microstructural level,

electron diffraction patterns were recorded from each using a Philips CM200 transmission electron microscope operating at 200 kV.

Magnetic measurements were carried out on finely ground powder samples using a Quantum Design MPMS 5000 SQUID magnetometer. The magnetization (M) was measured as a function of temperature on warming from 2 to 300 K after cooling both in zero field (ZFC) and in the measuring field of 100 Oe (FC). The isothermal magnetization was measured as a function of field ($-50 \leqslant H$ (kOe) $\leqslant 50$) on selected samples after cooling to the measuring temperature in 50 kOe. The a.c. susceptibility of selected samples was measured in an oscillating field of 3.5 Oe and a static field of ~2 Oe. Data were recorded at selected frequencies ($1 \leqslant \omega$ (Hz) $\leqslant 1000$) over a relatively narrow temperature range in the region of interest using a temperature step size of 0.2 K ($x = 0.5$) or 0.1 K ($x = 0.1$, 1.0).

3. Results

3.1. Compositions prepared by the ceramic method

Monophasic samples of compositions in the range $0.1 \leqslant x \leqslant 0.7$ could be synthesized by the ceramic method; we were unable to prepare pure samples having $x = 0.0$, 0.9 and 1.0 in this way. The X-ray diffraction patterns of the pure products could be indexed in the tetragonal space group $I4/mmm$ with unit-cell parameters $a_{tet} \sim 3.8$ Å, $c_{tet} \sim 12.4$ Å, with the exception of the pattern collected from the composition $x = 0.1$. In this case the broadening of a particular subset of the Bragg reflections (for example 1 1 0 but not 1 0 3) indicated the presence of an orthorhombic distortion requiring a doubling of the unit-cell volume. Our subsequent Le Bail and Rietveld analyses showed that this composition can be described in a unit cell of size $\sim\sqrt{2}a_{tet} \times \sqrt{2}a_{tet} \times c_{tet}$ in space group $Fmmm$, with the two reflections mentioned above indexing as 2 0 0 and 1 1 3. The reflections in the diffraction patterns of the other compositions were not broadened beyond the instrumental resolution. The unit-cell parameters of the compositions made by the ceramic method are listed in Table 1.

3.2. Compositions prepared by the solution method

Monophasic samples of compositions in the range $0.5 \leqslant x \leqslant 1.0$ could be prepared by the solution method. Samples having $x < 0.5$ contained small quantities of $n = \infty$ perovskites and/or other oxides in addition to the main $n = 1$ phase. The use of slower cooling rates or complete furnace cooling did not appear to affect the phase purity of the samples or the distribution of the cations over the A and B sites. The X-ray diffraction patterns of the pure samples $x = 0.5$, 0.75 and 1.0 could be indexed in the tetragonal space group $I4/mmm$. The derived unit-cell parameters are included in Table 1.

Table 1
Unit cell parameters of $Pr_{3-x}Sr_{1+x}CrNiO_8$ at room temperature

x	Space group	a (Å)	b (Å)	c (Å)	V (Å^3)[a]
0.1	*Fmmm*	5.45003(8)	5.44137(8)	12.3547(2)	183.194(7)
0.2	*I4/mmm*	3.84294(4)	–	12.3814(1)	182.851(5)
0.3	*I4/mmm*	3.83613(6)	–	12.4043(2)	182.541(9)
0.4	*I4/mmm*	3.83113(4)	–	12.4249(1)	182.367(6)
0.5	*I4/mmm*	3.82673(5)	–	12.4425(2)	182.206(7)
0.5[b]	*I4/mmm*	3.82661(3)		12.4441(5)	182.218(7)
0.6	*I4/mmm*	3.82301(3)	–	12.4600(1)	182.108(5)
0.7	*I4/mmm*	3.81921(7)	–	12.4760(2)	181.980(9)
0.75[b]	*I4/mmm*	3.81730(2)		12.4839(1)	181.913(5)
1.0[b]	*I4/mmm*	3.80916(3)	–	12.5172(1)	181.621(3)

[a] Volume per formula unit.
[b] Prepared from solution; unmarked samples by the ceramic method.

3.3. Transmission electron microscopy

Typical electron diffraction patterns taken along the [001], [010] and [110] zone axes of both samples having the composition $x = 0.5$ are shown in Fig. 2. There is no apparent difference between the sample prepared by the ceramic route and that prepared from solution. Neither sample shows evidence of superlattice formation along the principal lattice directions, i.e. ⟨100⟩, ⟨110⟩ and ⟨0 0 1⟩.

3.4. Magnetometry

The temperature dependence of the d.c. molar magnetic susceptibility (defined as $\chi = M/H$) of representative samples ($x = 0.1$, 0.5, 1.0) is plotted in Fig. 3. The data shown for the composition $x = 0.5$ were actually collected on the ceramic sample, but the sample made by the solution method gave essentially identical results. The ZFC susceptibility of each sample shows a local maximum at low temperature (T_f) and appears to follow a Curie–Weiss law, parameterized by the molar Curie constant, C_m, and the Weiss constant, θ, at higher temperatures. The values of T_f, C_m and θ are given in Table 2. The value of T_f decreases with increasing Sr content; θ is negative for all the compositions studied and becomes more so with increasing Sr content. The ZFC and FC susceptibilities are equal above T_f for all compositions other than $x = 0.1$, where some hysteresis is observed at temperatures up to 150 K. Below T_f the ZFC and FC susceptibilities behave differently. For all compositions having $x > 0.2$ the ZFC data show a positive temperature gradient below T_f, although a broad shoulder is apparent below T_f (at ~7 K when $x = 0.5$ and ~9 K when $x = 1.0$). When $x \leqslant 0.2$ the ZFC susceptibility has a negative temperature gradient at the lowest temperatures measured. The temperature gradient of the FC susceptibility changes at T_f, but remains negative throughout the measured temperature range for all compositions; no maximum is observed.

The field dependence of the magnetization is shown for selected samples in Fig. 4. At 2 K hysteresis is clearly apparent, particularly in low (<2000 Oe) applied fields. However, at temperatures between T_f and the broad shoulder in the temperature dependence of the susceptibility the hysteresis, although still present, is much reduced.

The temperature dependence of the real a.c. susceptibility of the compositions $x = 0.1$, 0.5 and 1.0 is shown in Fig. 5. The real component of the susceptibility of the compositions $x = 0.5$ and 1.0 passes through a maximum at a frequency-dependent temperature close to that reported as T_f in Table 2; the susceptibility is frequency dependent at temperatures below the maximum. The frequency dependence of the transition temperature can be described using the parameter $\Delta T_f/[T_f \Delta(\log \omega)]$, which reflects the change in the transition temperature with the logarithmic change in frequency [13]. This parameter takes the values 0.011 and 0.015 respectively for the compositions $x = 0.5$ and 1.0. In the case of $x = 0.1$, the real component of the susceptibility is frequency dependent both above and below T_f, although any frequency dependence of T_f is too small to be identified in our data. The behaviour of the imaginary components of the susceptibilities in the region of T_f is shown in Fig. 6. Although this component is very weak, a maximum is apparent in the region of T_f for each sample; this is most obvious in the data collected at relatively low frequencies.

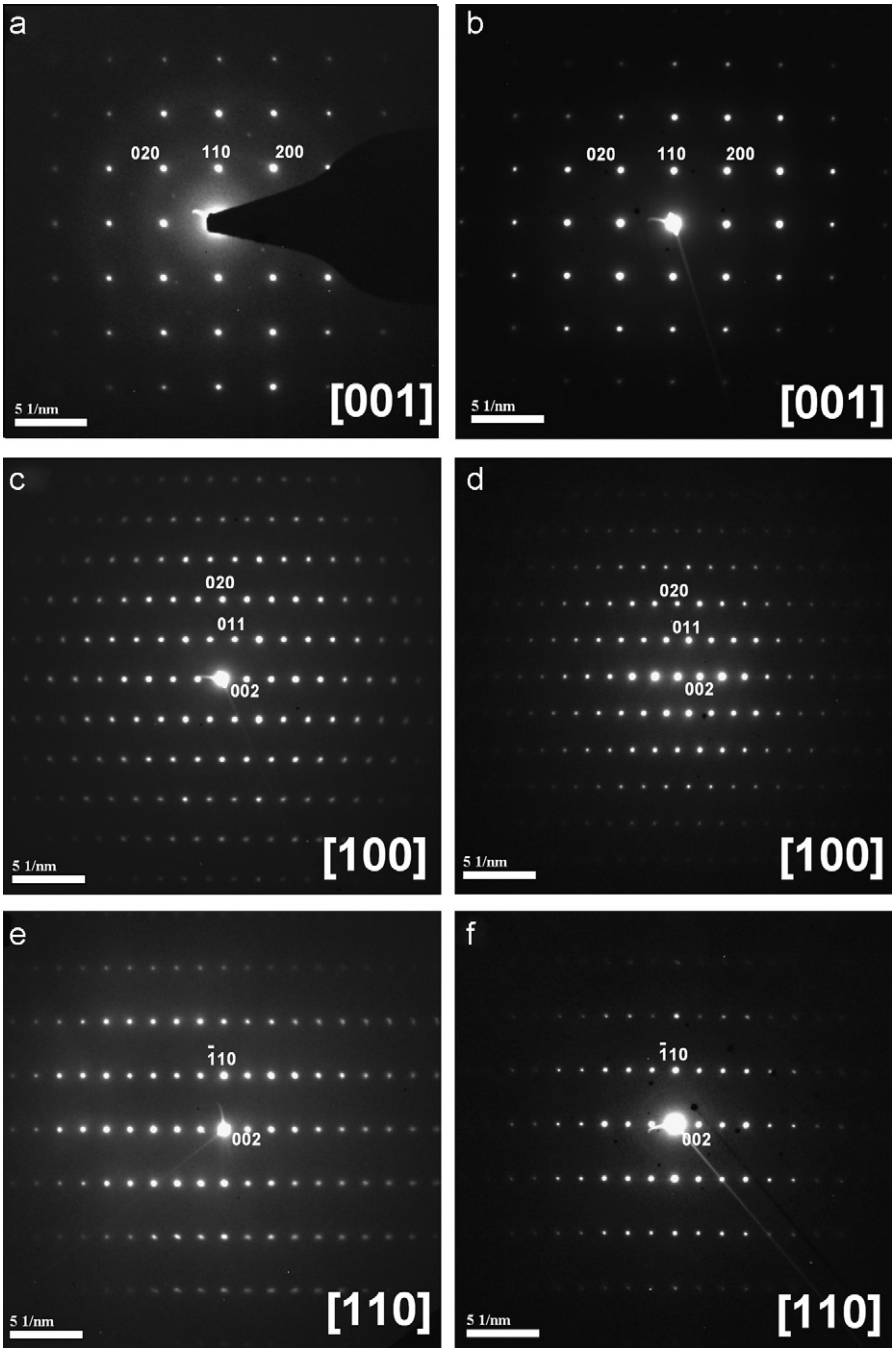

Fig. 2. Electron diffraction patterns taken along the (a, b) [001], (c, d) [100] and (e, f) [110] zone axes of $Pr_{2.5}Sr_{1.5}CrNiO_8$ prepared by (a, c, e) the ceramic method and (b, d, f) a solution method.

3.5. Neutron diffraction

The neutron diffraction patterns recorded at 5 K on samples of the compositions $x = 0.1$ and 1.0 showed no major intensity changes or additional peaks when compared with those collected at room temperature. They were therefore analysed under the assumption that no long-range magnetic order was present in either sample at 5 K. Rietveld analysis of the data proceeded smoothly in space group *Fmmm* ($x = 0.1$) or *I4/mmm* ($x = 1.0$). The resulting structural parameters are listed in Tables 3 and 4 and the fitted profiles are shown in Figs. 7 and 8. The corresponding bond lengths are given in Table 5. Preliminary refinements in which the occupation factors of the O1 and O2 sites were allowed to vary provided no evidence for the presence of anion vacancies and these parameters were subsequently constrained to be unity.

4. Discussion

The results described above show that the ceramic and solution synthesis methods are suited to different ranges of composition in the system $Pr_{3-x}Sr_{1+x}CrNiO_8$. The former was able to access Pr-rich compositions ($0.1 \leqslant x \leqslant 0.7$), whereas the latter lead to the synthesis of monophasic Sr-rich compositions ($0.5 \leqslant x \leqslant 1.0$). Larger homogeneous samples could be prepared by the solution method; this is the reason for the difference between the intensity scales of Figs. 7 and 8. One composition,

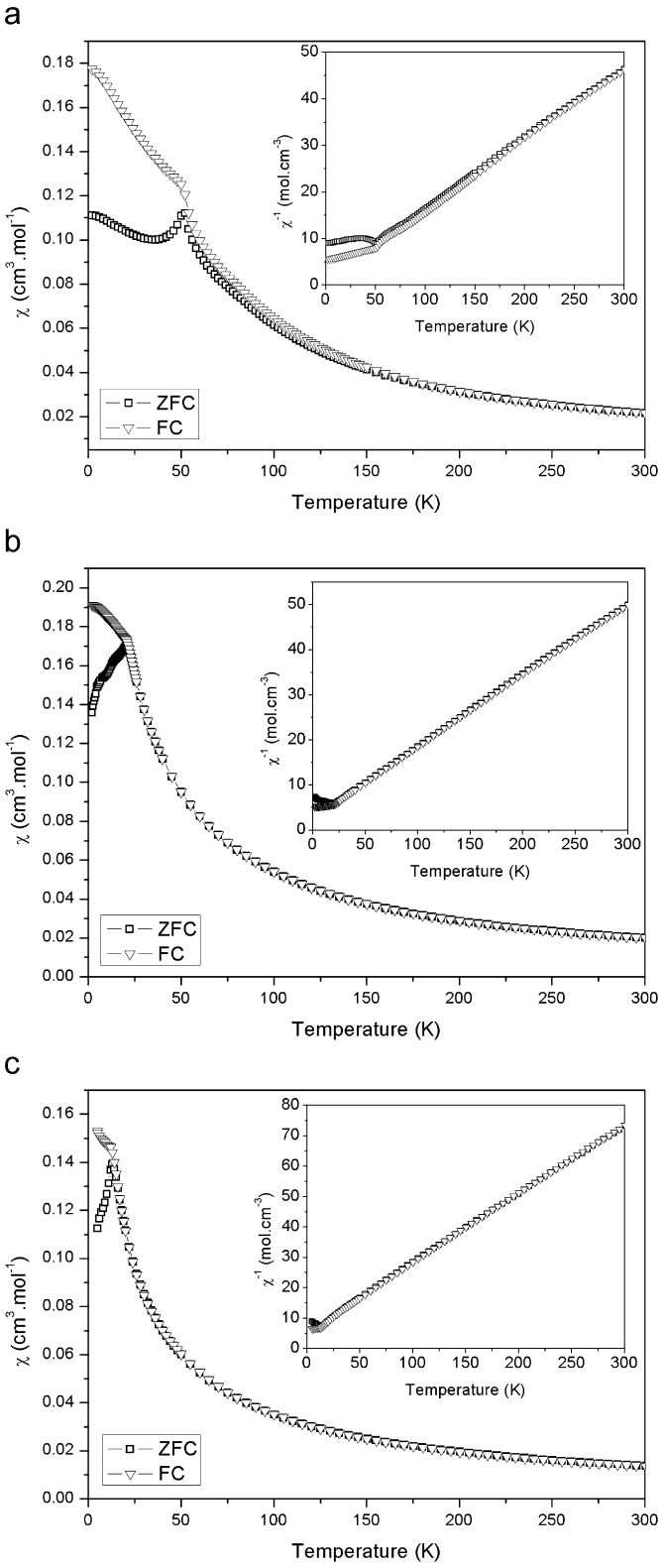

Fig. 3. Temperature dependence of the molar d.c. magnetic susceptibility of $Pr_{3-x}Sr_{1+x}CrNiO_8$ measured in 100 Oe for $x = $ (a) 0.1, (b) 0.5 and (c) 1.0. The inverse susceptibility is inset.

$Pr_{2.5}Sr_{1.5}CrNiO_8$, was prepared by both methods; the results of our experiments on the two samples showed that both their microstructural and their bulk characteristics were essentially identical, thus demonstrating that the use of different preparative methods does not limit our discussion of the properties as a function of composition.

Table 2
Magnetic parameters of $Pr_{3-x}Sr_{1+x}CrNiO_8$

x	T_f (K)	C_m (emu)	θ (K)
0.1	52 (1)	6.63 (4)	−9.0 (1)
0.2	40 (1)	6.59 (1)	−8.7 (2)
0.3	30 (2)	6.43 (1)	−12.0 (2)
0.4	26 (1)	6.23 (1)	−12.3 (2)
0.5	21.0 (3)	6.27 (1)	−15.7 (2)
0.6	16.0 (5)	6.05 (5)	−17.8(5)
0.7	14 (1)	6.15 (1)	−20.8 (1)
0.75	13.2 (1)	5.76 (1)	−20.6 (1)
1.0	13.0 (5)	4.39 (1)	−23.3 (2)

The $n = 1$ RP crystal structure is preserved across the composition range, although an orthorhombic distortion is observed in the most Pr-rich composition ($x = 0.1$). The absence of superlattice reflections in the X-ray and neutron diffraction patterns proves that there is no long-range ordering of the Cr and Ni cations in any composition. The absence of superlattice reflections and diffuse streaking from the electron diffraction patterns taken along three zone axes shows that three-dimensional cation ordering does not occur at the microstructural level, at least in the composition $x = 0.5$, and that there is no two-dimensional ordering within the perovskite-like sheets [8,14]. Substitution of Pr^{3+} by Sr^{2+} might be expected to lead to an increase in unit-cell volume but in fact the opposite trend is observed (Table 1); a steady increase in c with increasing x is more than compensated by the concomitant decrease in a. The value of the latter parameter is simply determined by the mean B–O distance in the xy plane and the steady decrease observed strongly suggests that the charge mismatch brought about by the replacement of Pr^{3+} by Sr^{2+} is compensated by the oxidation of Ni^{2+} to Ni^{3+}, rather than by the oxidation of residual Pr^{3+} to Pr^{4+}. Furthermore, the length of the B–O bond parallel to the z-axis also decreases with increasing Sr content, thus maintaining a near-constant value (~1.05) for the ratio $(B\text{–O})_z/(B\text{–O})_{xy}$. Ni^{3+} therefore behaves as a spherical cation when replacing Ni^{2+}; there is no evidence for a cooperative Jahn–Teller effect in the disordered cation array and no long-range orbital ordering is apparent. The most obvious structural change attributable to the relatively large size and low charge of Sr^{2+} is thus the increase in the separation between the sheets of octahedra, as is illustrated by the increase in the mean length of the Pr/Sr–O1 bond lying parallel to [001] from 2.314(3) ($x = 0.1$) to 2.369(2) ($x = 1.0$). The increase in length of this bond is of course compatible with the shortening of the axial Cr/Ni–O1 bond that occurs when Ni^{2+} is oxidized to Ni^{3+}, and suggests that the introduction of Sr^{2+} increases the two-dimensional character of the system. The refined values of the anisotropic atomic displacement parameters (Tables 3 and 4) suggest that the O1 and O2 anions in both compositions respond to the different sizes of the B-site cations by disordering in the xy plane rather than parallel to z.

Neutron diffraction and X-ray absorption spectroscopy have previously shown [15,16] that the cation oxidation states in $PrNiO_3$ are Pr^{3+} and Ni^{3+}, as we have proposed above for the $Pr_{3-x}Sr_{1+x}CrNiO_8$ system. The formation of a Ni^{3+} compound under an argon atmosphere might at first sight seem surprising given that Strangfeld et al. [17] were unable to prepare Ni^{3+}-rich samples of $(La_{1-x}Sr_x)_2NiO_{4+\delta}$ without the use of high oxygen pressure. Millburn and Rosseinsky [18] have previously argued that the Cr^{3+} cations, having a relatively low electronegativity, do not compete strongly with Ni^{3+} for the negative charge on the anion, and that the charge on the latter cations is consequently

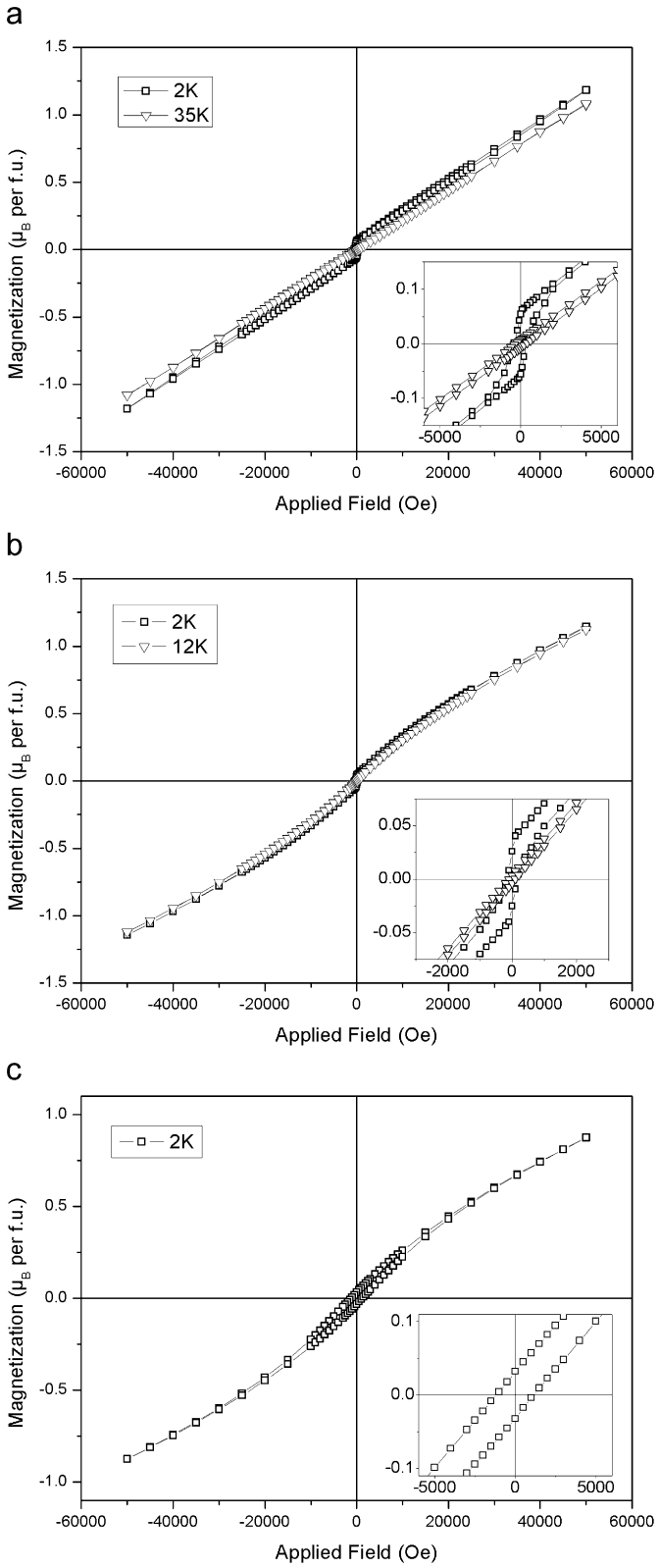

Fig. 4. Field dependence of the magnetization per formula unit of $Pr_{3-x}Sr_{1+x}CrNiO_8$ at selected temperatures: $x = (a)$ 0.1, (b) 0.5 and (c) 1.0.

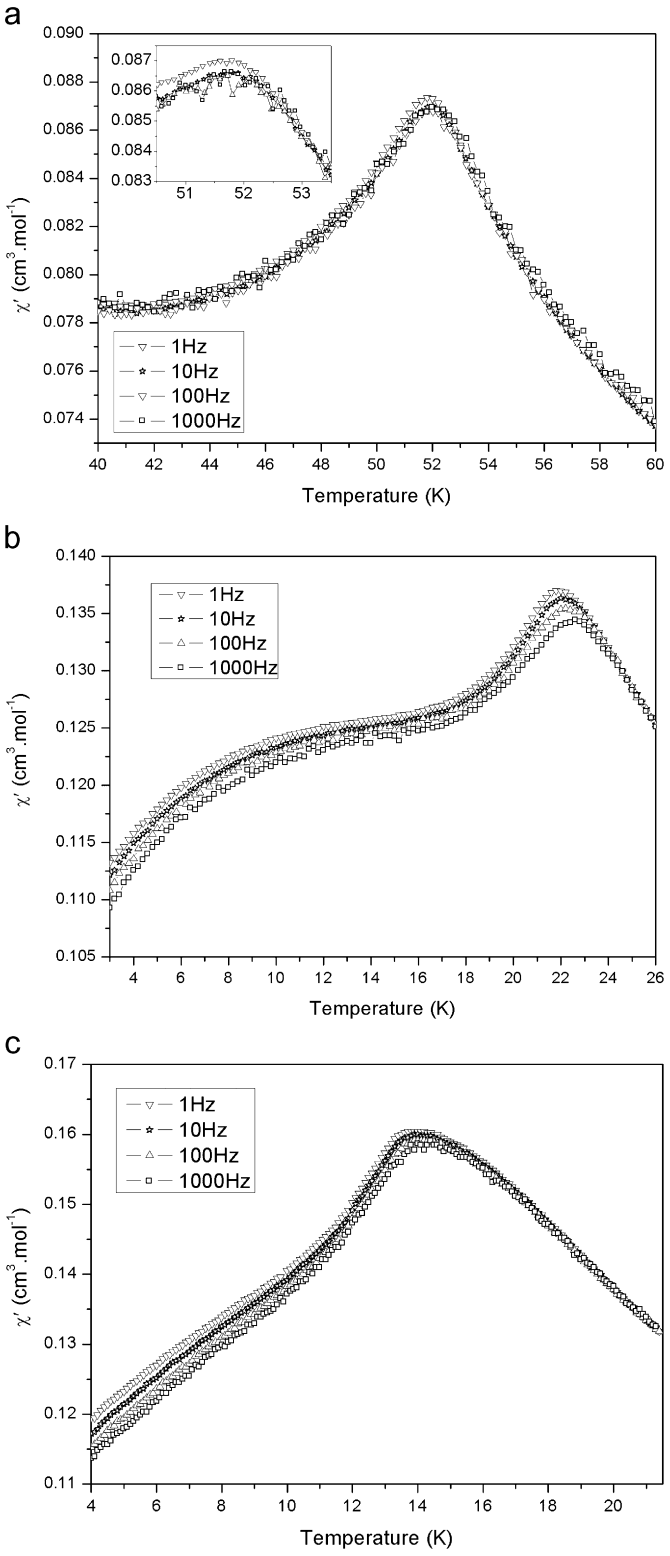

Fig. 5. Real part of the molar a.c. magnetic susceptibility of $Pr_{3-x}Sr_{1+x}CrNiO_8$ as a function of temperature and frequency: $x = (a)$ 0.1, (b) 0.5 and (c) 1.0.

stabilized by covalent bonding. XANES could be used to determine directly the oxidation states of the cations in the $Pr_{3-x}Sr_{1+x}CrNiO_8$ system.

The structural behaviour described above is compatible with that seen in related compounds. The lower symmetry space group adopted by $Pr_{2.9}Sr_{1.1}CrNiO_8$ permits neither tilting of the BO_6 octahedra nor atomic displacements; it simply removes the requirement for the unit-cell parameters in the *xy* plane to be identical. It is likely that the distortion occurs in order to relieve the strain induced when the average size of the *A*-site cations falls below a critical value. $La_2NiO_{4+\delta}$ has also been reported to adopt

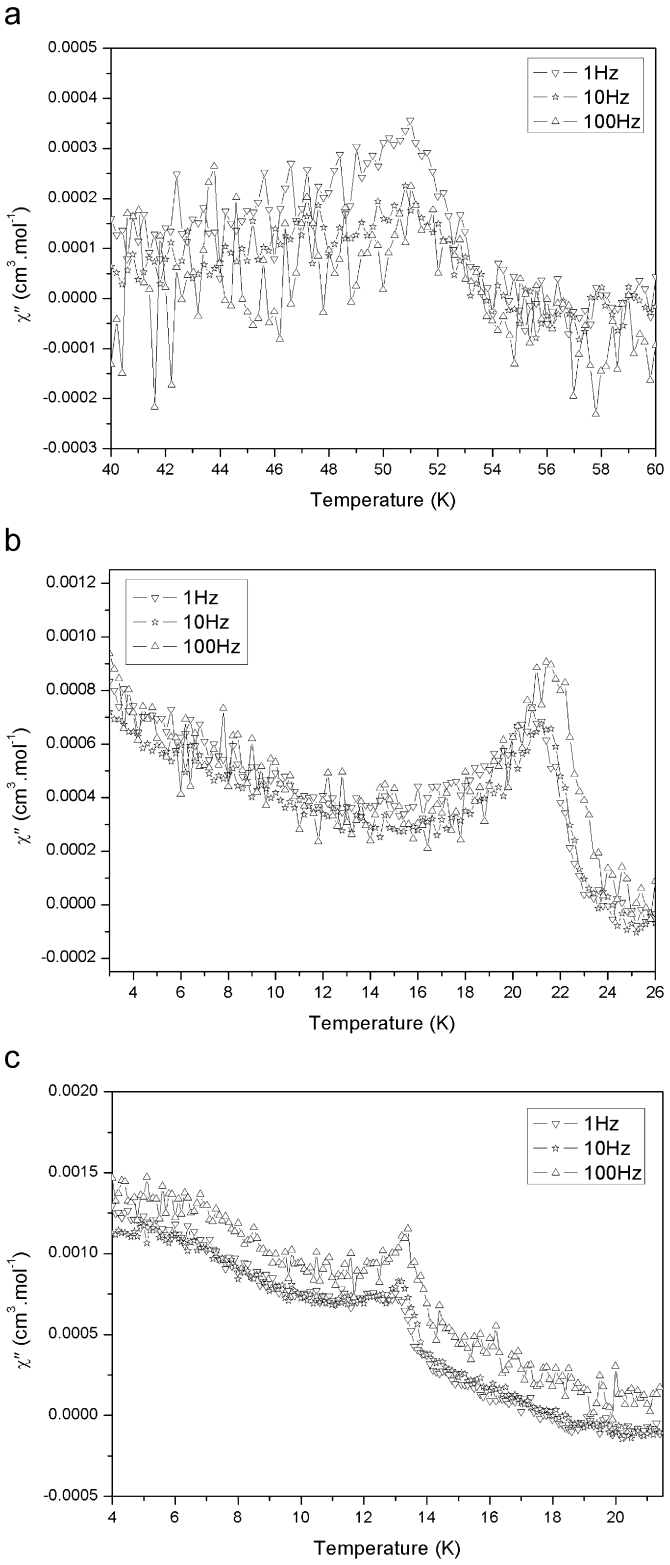

Fig. 6. Imaginary part of the molar a.c. magnetic susceptibility of $Pr_{3-x}Sr_{1+x}$ $CrNiO_8$ as a function of temperature and frequency: x = (a) 0.1, (b) 0.5 and (c) 1.0.

the space group *Fmmm* [19], although the orthorhombic distortion was closely linked to the presence of excess oxygen; we did not detect any such excess in the analysis of neutron diffraction data collected on $Pr_{2.9}Sr_{1.1}CrNiO_8$. $Pr_2NiO_{4+\delta}$ has also been described in *Fmmm*, with replacement of Pr^{3+} by Ba^{2+} [20] resulting in a

Table 3
Structural parameters of $Pr_{2.9}Sr_{1.1}CrNiO_8$ at 5 K

a (Å)		5.42583(6)
b (Å)		5.41481(6)
c (Å)		12.2934(1)
V^a (Å^3)		180.589(7)
R_{wp}		0.0596
Pr/Sr	z	0.3604(2)
	B_{iso} (Å^2)	0.29(4)
Cr/Ni	β_{11}	0.0015(11)
	β_{22}	0.0027(10)
	β_{33}	0.0001(2)
O1	z	0.17226(2)
	β_{11}	0.0168(12)
	β_{22}	0.0129(11)
	β_{33}	0.0007(2)
O2	β_{11}	0.0012(8)
	β_{22}	0.0047(9)
	β_{33}	0.0018(2)
	β_{12}	−0.0007(5)

Space group *Fmmm*. Pr/Sr on 0 0 z, Cr/Ni on 0 0 0, O1 on 0 0 z and O2 on $\frac{1}{4}\frac{1}{4}0$.
[a] Volume per formula unit.

Table 4
Structural parameters of $Pr_2Sr_2CrNiO_8$ at 5 K

a (Å)		3.79129(1)
c (Å)		12.4606(6)
V^a (Å^3)[a]		179.107(1)
R_{wp}		0.0542
Pr/Sr	z	0.3583(1)
	B_{iso} (Å^2)	0.08(2)
Cr/Ni	β_{11}	−0.0003(5)
	β_{22}	−0.0003(5)
	β_{33}	−0.0005(10)
O1	Z	0.1682(1)
	β_{11}	0.0151(5)
	β_{22}	0.0151(5)
	β_{33}	0.0009(1)
O2	β_{11}	0.0056(8)
	β_{22}	0.0067(8)
	β_{33}	0.0005(1)

Space group *I*4/*mmm*. Pr/Sr on 0 0 z, Cr/Ni on 0 0 0, O1 on 0 0 z and O2 on $\frac{1}{2}00$.
[a] Volume per formula unit.

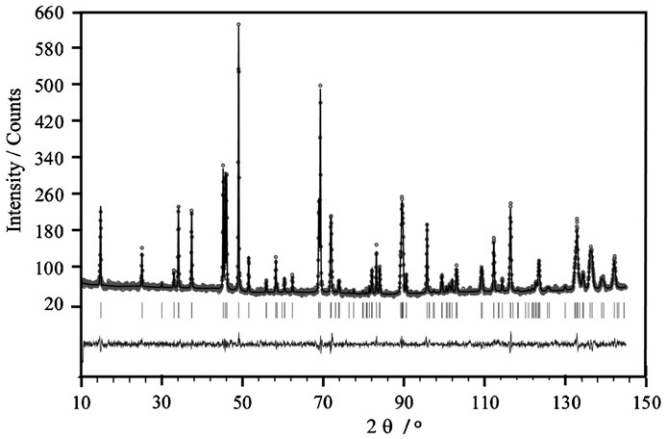

Fig. 7. Observed (o) and calculated (−) neutron diffraction profiles for $Pr_{2.9}Sr_{1.1}CrNiO_8$ at 5 K; a difference curve is also shown. Reflection positions are indicated by vertical lines.

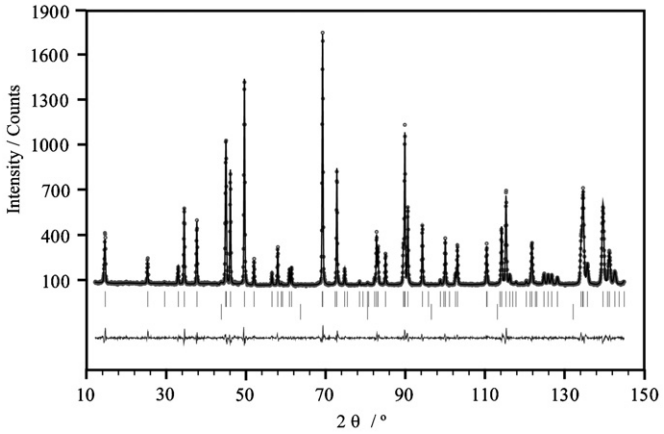

Fig. 8. Observed (o) and calculated (−) neutron diffraction profiles for $Pr_2Sr_2CrNiO_8$ at 5 K; a difference curve is also shown. Reflection positions for the RP phase (upper) and the vanadium sample container (lower) are indicated by vertical lines.

Table 5
Bond lengths (in Å) in $Pr_{2.9}Sr_{1.1}CrNiO_8$ and $Pr_2Sr_2CrNiO_8$ at 5 K

	$Pr_{2.9}Sr_{1.1}CrNiO_8$	$Pr_2Sr_2CrNiO_8$
Cr/Ni–O1	2.117(2) × 2	2.0957(17) × 2
Cr/Ni–O2	1.916374(3) × 4	1.8956455(1) × 4
Mean Cr/Ni	1.983	1.962
Pr/Sr–O1	2.314(3) × 1 2.7424(5) × 2 2.7369(5) × 2	2.369(2) × 1 2.7011(3) × 4
Pr/Sr–O2	2.5725(16) × 4	2.5904(10) × 4
Mean Pr/Sr	2.618	2.615

transition to the tetragonal space group *I*4/*mmm*, which is also observed for $PrSrCrO_4$ [21]. The phase transition that occurs in the system $Pr_{2-x}Ba_xNiO_{4+\delta}$ as Ni^{2+} is oxidized to Ni^{3+} provides a parallel with the behaviour of $Pr_{3-x}Sr_{1+x}CrNiO_8$, which we have shown to undergo a transition from orthorhombic to tetragonal symmetry when the concentration of Sr^{2+} increases above 27.5%. However, it should be noted that the space-group assignment of $Pr_2NiO_{4+\delta}$ is not unambiguous, and the orthorhombic group *Bmab* has been assigned [22] to the $\delta = 0$ composition on the basis of a powder neutron diffraction experiment carried out on a sample that had been reduced under hydrogen. Sullivan et al.[23] have subsequently shown that the space-group symmetry is strongly dependent on the oxygen excess, as parameterized by δ.

The failure of the transition-metal cations to adopt an ordered distribution over the six-coordinate sites must be attributable to the relative size and charge of the species involved. Ordering was most likely to occur in the Pr-rich, and hence Ni^{2+}-rich, compositions where the size and charge difference is greatest ($r(Ni^{2+}) = 0.69$ Å, $r(Cr^{3+}) = 0.615$ Å [24]), but this clearly was not enough to have a dominating influence on the structure. It thus remains the case that if two different elements order over the *B* sites of an $n = 1$ RP structure, one of the relatively large Li^+ [8,9,25–28], Mg^{2+} or Zn^{2+} [14,29] cations is usually involved ($r(Li^+) = 0.76$ Å, $r(Mg^{2+}) = 0.72$ Å, $r(Zn^{2+}) = 0.74$ Å). Even in these compounds the ordering is often incomplete or occurs only over relatively short distances. The charge ordering observed in mixed-valence systems based on a single element, for example $La_{2-x}Sr_xNiO_4$ [30], provides a marked contrast to this behaviour.

There are several points of interest among the magnetic parameters listed in Table 2. For example, the experimentally determined molar Curie constant (C_m) is always significantly lower than the value calculated assuming a full paramagnetic contribution from Pr^{3+} and spin-only contributions from the appropriate concentrations of Cr^{3+}, Ni^{2+} and low-spin Ni^{3+}. The discrepancy increases when high-spin Ni^{3+} or Ni^{2+}/Pr^{4+} are assumed to be present. The difference between the ZFC and FC susceptibilities of the composition $x = 0.1$ in the temperature range $50 < T$ (K) < 150 shows that this material is not truly paramagnetic at temperatures well above that of the maximum in χ_{ZFC}. We assume that the Pr^{3+} spins are paramagnetic in this region, and that the hysteresis and reduction in the Curie constant are the result of short-range interactions between the transition-metal cations. The simultaneous observation of a Weiss constant (θ) of −9 K and a maximum in χ_{ZFC} at $T_f = 52$ K provides further evidence of complex magnetic behaviour; in the case of an antiferromagnetic insulator the modulus of the Weiss constant would be expected to be significantly larger than the Néel temperature. The relative values of θ and T_f suggest that ferromagnetic and antiferromagnetic interactions of comparable strengths are present and that the competition between them results in the formation of a spin-glass phase at 52 K. This interpretation is consistent with the absence of magnetic Bragg scattering from the neutron diffraction pattern recorded at 5 K, although there is little evidence in the real part of the a.c. susceptibility for a frequency dependence in the value of T_f. However, χ' is frequency dependent even above T_f and an increase is observed in χ'' at T_f for the lowest measuring frequencies. The hysteresis observed in the d.c. susceptibility above T_f can be attributed to the formation of blocked spin-clusters above the freezing temperature [31], as can the frequency dependence of χ' in the same temperature range. We suggest that the onset of irreversibility well above the transition temperature might be the reason that T_f appears to be independent of frequency. The continued rise of χ_{FC} on cooling below T_f could be attributable to the presence of unfrozen spins in entropic spin clusters [32], or to the continued presence of paramagnetic spins below the transition temperature; the negative temperature gradient of χ_{ZFC} below ~40 K also suggests the presence of paramagnetic cations. These are most likely to be Pr^{3+} species. Comparison of the low-field hysteresis in the magnetization at 35 and 2 K reveals a significant enhancement of the remanent magnetization at the lower temperature, perhaps attributable to a change in the contribution from these cations.

In compositions with $x > 0.1$, neither hysteresis (d.c.) nor frequency dependence (a.c.) is observed in the magnetic susceptibility above T_f. C_m and T_f decrease with increasing strontium content and the value of θ becomes more negative. The latter observation suggests an increasing dominance by the antiferromagnetic interactions. The reduction in T_f is probably a consequence of the increasing separation of the perovskite-like layers as the strontium concentration increases. This, together with the replacement of paramagnetic Pr^{3+} by diamagnetic Sr^{2+}, has the effect of weakening the superexchange interactions along [001], thus increasing the two-dimensional character of the structure. Over the composition range $0.1 < x \leqslant 1.0$, χ_{ZFC} only shows a negative gradient below T_f in the case of $Pr_{2.8}Sr_{1.2}CrNiO_8$. As the Sr content increases a second transition is observed below T_f; the d.c. susceptibility data for $x = 0.5$, presented in Fig. 3(b), show a maximum in χ_{ZFC} at $T_f = 21$ K, and clear evidence of a second transition at ~7 K. The real part of the a.c. susceptibility clearly shows the value of T_f to be frequency dependent, and there is an increase in the imaginary component at the transition temperature; the value of the parameter $\Delta T_f/[T_f \Delta(\log \omega)]$ is similar to those observed for other insulating spin glasses. We therefore assign this as a transition to a spin-glass state. The gradient of χ' becomes steeper below ~10 K, as does that of χ_{ZFC}. We suggest that this

change marks the onset of freezing on the Pr^{3+} sublattice. Further evidence for this assignment comes from the marked change in $M(H)$ between 12 and 2 K. There is thus a clear difference in the behaviour of the compositions $x = 0.1$ and 0.5 in that we see evidence in the susceptibility of the latter for a second magnetic transition, possibly attributable to the Pr^{3+} sublattice, whereas in the more Pr-rich sample we saw no direct evidence, despite an increase in the remanent magnetization between 35 and 2 K. The imaginary component of the a.c. susceptibility is larger below T_f for the more Sr-rich samples, which suggests that more complex spin dynamics are operating; we cannot be more specific with the limited data presently available. The decrease in T_f continues for $x > 0.5$, reaching a value of ~13 K for $x \geqslant 0.7$. In the composition $Pr_2Sr_2CrNiO_8$, containing only Ni^{3+}, χ_{ZFC} shows evidence of a second transition at ~10 K. Taken together, the absence of magnetic Bragg scattering in the neutron diffraction pattern at 5 K, the temperature dependence of χ_{ZFC} and χ_{FC} in the d.c. susceptibility data and the frequency dependence of T_f in the a.c. susceptibility data provide strong evidence that this composition can also be considered as a spin glass. In our introductory remarks we explained how the absence of cation ordering might result in spin-glass behaviour as a consequence of competition between antiferromagnetic B–O–B interactions and ferromagnetic B–O–B' interactions. However, we should also recognize that spin-glass behaviour has been reported in $(La_{1-x}Sr_x)_2NiO_4$ [17], and that we cannot attribute all the frustration to the presence of both Cr^{3+} and Ni^{2+}/Ni^{3+} in the structure; the interactions between Ni^{2+} and Ni^{3+} may be a contributory factor. We note that, in the absence of competing interactions, the Cr^{3+} sublattice of $PrCaCrO_4$ orders antiferromagnetically at ~180 K, and that the effective magnetic moment in the temperature range $200 \leqslant T\,(K) \leqslant 300$ is significantly reduced from the free-ion value; this reduction has been ascribed to two-dimensional correlations within the perovskite-like layers [33]. The Pr^{3+} cations on the A sites remain paramagnetic down to 40 K, at which point the gradient of $\chi(T)$ decreases markedly. However, these cations do not contribute to the magnetic Bragg scattering observed at 1.5 K. The Ni^{2+} sublattice in Pr_2NiO_4 is antiferromagnetically ordered below 325 K [34] and the Pr^{3+} spins are reported to be polarized below 40 K. The behaviour of Pr_2NiO_4, but not that of $PrCaCrO_4$, thus supports our suggestion that the Pr^{3+} spins couple sufficiently strongly to the transition-metal sublattice in $Pr_{3-x}Sr_xCrNiO_8$ to freeze below T_f.

The results described above can be compared with those reported in previous studies of mixed-cation $n = 1$ RP phases. A number of related studies of the $Ln_2A'_2MnNiO_8$ ($A' = Ca$, Sr; $Ln = La$, Pr, Nd, Sm, Gd) have been carried out [35–37], but the most direct comparison available is perhaps with the study of $LaSrCr_xNi_{1-x}O_{4+\delta}$ by Millburn and Rosseinsky [18]. They showed that $LaSrCr_{0.5}Ni_{0.5}O_4$, synthesized by a sol–gel method, adopts a tetragonal structure (space group $I4/mmm$) with disordered distributions of La/Sr cations on the A sites and Cr^{3+}/low-spin Ni^{3+} cations on the B sites. The unit-cell parameters of $LaSrCr_{0.5}Ni_{0.5}O_4$ are, not surprisingly, longer than those of the Pr analogue, but the strain within the octahedra, defined as the ratio of the difference and the sum of the axial and equatorial Cr/Ni–O bond lengths, is very similar in the two compositions (0.050 for $Pr_2Sr_2CrNiO_8$). Magnetometry revealed a transition to a spin-glass phase on cooling below 16 K. In the absence of a magnetic cation on the A sites, there was no evidence for a second magnetic transition below T_f. These results are apparently consistent with those reported above for $Pr_2Sr_2CrNiO_8$. However, on closer inspection of the data some inconsistencies appear. The Weiss temperature of $LaSrCr_{0.5}Ni_{0.5}O_4$ was found to be −2.17 K and the molar Curie constant (normalized to $La_2Sr_2CrNiO_8$) was 2.12 $cm^3\,K\,mol^{-1}$. The former value implies that the antiferromagnetic interactions are more dominant in our Pr-containing material. If we assume that Pr^{3+} has an effective free-ion magnetic moment of 3.58 μ_B, then the contribution by the B-site cations to the observed Curie constant (4.39 $cm^3\,K\,mol^{-1}$) is only ~1.2 $cm^3\,K\,mol^{-1}$, approximately half of the value determined for the La-containing compound. We drew attention to this shortfall in a less quantitative manner above. This implies either that the Pr^{3+} cations are more strongly influenced by crystal field effects than might have been expected or that extensive short-range antiferromagnetic coupling is present throughout the measured temperature range. The latter explanation seems more likely, in which case the apparently linear temperature dependence of the inverse susceptibility above T_f is fortuitous and misleading, and the use of the Curie–Weiss law to model these data is not valid. Although Millburn and Rosseinsky focus principally on La/Sr-containing phases they do make brief mention of $Nd_2Ca_2CrNiO_8$. They describe the magnetism of Nd^{3+} as swamping that of the transition metals, such that the freezing of the spins of the latter appears only as a point of inflection in the temperature dependence of the susceptibility. This is clearly very different from the behaviour of $Pr_2Sr_2CrNiO_8$, illustrated in Fig. 3(c), where no further increase in χ_{ZFC} is observed on cooling below T_f and where we have assigned the change in gradient at ~10 K to a freezing of the Pr^{3+} moments. It is not obvious why the two systems behave differently, but this does emphasize that the magnetic properties are sensitive to the properties of all the chemical elements present, and not just to those of the elements on the primary magnetic sublattice. We are investigating the role of the lanthanide cation more thoroughly in an on-going study of compounds in the series $Nd_{3-x}Sr_{1+x}CrNiO_8$.

The $Ln_xSr_{2-x}Mn_{0.5}Cu_{0.5}O_4$ ($Ln = La$, Nd, Pr) system has been characterized by McCabe and Greaves [38]. This is one of the few previous studies to report a detailed assessment of the consequences of varying the relative concentration of the lanthanide and alkaline earth cations whilst maintaining a 1:1 of two transition metals in the $n = 1$ RP structure. As in the case of $Pr_{3-x}Sr_{1+x}CrNiO_8$, the transition-metal cations do not order over the six-coordinate sites. Both $LaSrMn_{0.5}Cu_{0.5}O_4$ and $La_{1.5}Sr_{0.5}Mn_{0.5}Cu_{0.5}O_4$ were shown to be antiferromagnetically ordered at low temperature, albeit with very low ordered magnetic moments on the cations. For example in $LaSrMn_{0.5}Cu_{0.5}O_4$, assumed to contain Cu^{2+} and Mn^{4+}, the atomic moments are defined to be $\mu_{Cu} = 0.31(3)$ and $\mu_{Mn} = 0.92(9)\,\mu_B$. The magnetic susceptibility of both compositions showed a complex temperature dependence that resulted in an explanation involving the antiferromagnetic alignment of ferromagnetic clusters. $PrSrMn_{0.5}Cu_{0.5}O_4$ and $NdSrMn_{0.5}Cu_{0.5}O_4$ also show long-range antiferromagnetic order below ~100 K, but with positive values of the Weiss temperature suggesting that significant ferromagnetic coupling was also present. As in the case of $Pr_{3-x}Sr_{1+x}CrNiO_8$, the effective magnetic moment in the paramagnetic phase was significantly lower than the calculated value. In contrast to $Pr_{3-x}Sr_{1+x}CrNiO_8$, the lanthanide cations appear to remain paramagnetic throughout the measured temperature range. Rather than facilitating the interpretation of our own data, these results emphasize the complexity and diversity of the $n = 1$ RP systems.

In conclusion, we have shown that compositions in the system $Pr_{3-x}Sr_{1+x}CrNiO_8$ can be synthesized for $0.1 \leqslant x \leqslant 1.0$ provided that different synthetic methods are used to access different parts of the composition range. The data suggest that the cations are in the oxidation states Pr^{3+}, Cr^{3+} and Ni^{2+}/Ni^{3+}, the ratio of the latter two species being a function of x. No superlattice peaks indicative of cation ordering on either the Pr/Sr or the Ni/Cr sublattice are observed in the diffraction patterns. The results of our magnetometry experiments are complex and suggest that the disorder on the B-site cation sublattice gives rise to competing ferromagnetic and antiferromagnetic superexchange interactions, resulting in

the formation of a spin-glass state at low temperatures. There is evidence to suggest that the spins on the Pr^{3+} sublattice also freeze at the lowest temperatures. The absence of magnetic Bragg peaks in the neutron diffraction data collected from the samples having $x = 0.1$ and 1.0 at 5 K proves that no long-range magnetic order is present in these two limiting compositions. We attribute the apparent absence of magnetic ordering throughout the series to the absence of cation ordering on the six-coordinate sites. Controlling the cation distribution in $n = 1$ RP phases without diluting the magnetic sublattice by the introduction of diamagnetic Li^+, Mg^{2+} or Zn^{2+} thus remains a challenge for solid-state chemists. We remain convinced that the problem can be solved if the correct combination of cations is selected for both the *A* and the *B* sites.

Acknowledgments

We thank the British Council and Le Ministère des Affaires Etrangères et Européennes for financial support under the Alliance programme. We are grateful to E. Suard (ILL), T. Roisnel, T. Guizouarn and T. Bataille (Rennes) for experimental assistance and advice.

References

[1] J.B. Goodenough, P.M. Raccah, J. Appl. Phys. 36 (1965) 1031.
[2] E.J. Cussen, M.J. Rosseinsky, P.D. Battle, J.C. Burley, L.E. Spring, J.F. Vente, S.J. Blundell, A.I. Coldea, J. Singleton, J. Am. Chem. Soc. 123 (2001) 1111.
[3] M.A. Subramanian, B.H. Toby, A.P. Ramirez, W.J. Marshall, A.W. Sleight, G.H. Kwei, Science 273 (1996) 81.
[4] A.P. Ramirez, J. Phys.: Condens. Matter 9 (1997) 8171.
[5] J.B. Goodenough, Magnetism and the Chemical Bond, Wiley, New York, 1963.
[6] M.T. Anderson, K.B. Greenwood, G.A. Taylor, K.R. Poeppelmeier, Prog. Solid State Chem. 22 (1993) 197.
[7] P.D. Battle, T.C. Gibb, C.W. Jones, F. Studer, J. Solid State Chem. 78 (1989) 281.
[8] J.C. Burley, P.D. Battle, D.J. Gallon, J. Sloan, C.P. Grey, M.J. Rosseinsky, J. Am. Chem. Soc. 124 (2002) 620.
[9] J.A. Rodgers, P.D. Battle, N. Dupre, C.P. Grey, J. Sloan, Chem. Mater. 16 (2004) 4257.
[10] H.M. Rietveld, J. Appl. Crystallogr. 2 (1969) 65.
[11] A.C. Larson, R.B. von-Dreele, General Structure Analysis System (GSAS), LAUR 86-748, Los Alamos National Laboratories, 1994.
[12] J. Rodriguez-Carvajal, Physica B 192 (1993) 55.
[13] J.A. Mydosh, Spin Glasses: An Experimental Introduction, Taylor & Francis, London, 1993.
[14] J.C. Burley, P.D. Battle, P.J. Gaskell, M.J. Rosseinsky, J. Solid State Chem. 168 (2002) 202.
[15] J.L. Garcia-Munoz, J. Rodriguez-Carvajal, P. Lacorre, J.B. Torrance, Phys. Rev. B 46 (1992) 4414.
[16] M. Medarde, A. Fontaine, J.L. Garcia-Munoz, J. Rodriguez-Carvajal, M. de-Santis, M. Sacchi, G. Rossi, P. Lacorre, Phys. Rev. B 46 (1992) 14975.
[17] T. Strangfeld, K. Westerholt, H. Bach, Physica C 183 (1991) 1.
[18] J.E. Millburn, M.J. Rosseinsky, Chem. Mater. 9 (1997) 511.
[19] J.D. Jorgensen, B. Dabrowski, S. Pei, D.R. Richards, D.G. Hinks, Phys. Rev. B 40 (1989) 2187.
[20] Y.K. Chung, Y. Kwon, S.H. Byeon, Bull. Kor. Chem. Soc. 16 (1995) 120.
[21] J.C. Joubert, A. Collomb, D. Elmaleh, G.L. Flem, A. Daoudi, G. Ollivier, J. Solid State Chem. 2 (1970) 343.
[22] R. Saez-Puche, F. Fernandez, J. Rodriguez-Carvajal, J.L. Matinez, Solid State Commun. 72 (1989) 273.
[23] J.D. Sullivan, D.J. Buttrey, D.E. Cox, J. Hriljac, J. Solid State Chem. 94 (1991) 337.
[24] R.D. Shannon, Acta Crystallogr. A32 (1976) 519.
[25] S. Abou-Warda, W. Pietzuch, G. Berghofer, U. Kesper, W. Massa, D. Reinen, J. Solid State Chem. 138 (1998) 18.
[26] G. Demazeau, J.L. Marty, M. Pouchard, T. Rojo, J.M. Dance, P. Hagenmuller, Mater. Res. Bull. 16 (1981) 47.
[27] S.A. Warda, W. Massa, D. Reinen, Z. Hu, G. Kaindl, F.M.F.D. Groot, J. Solid State Chem. 146 (1999) 79.
[28] F. Abbattista, M. Vallino, D. Mazza, J. Less-Common Met. 110 (1985) 391.
[29] S.H. Byeon, G. Demazeau, J.H. Choy, Jpn. J. Appl. Phys. 34 (1995) 6156.
[30] S.W. Cheong, H.Y. Hwang, C.H. Chen, B. Batlogg, L.W. Rupp, Jr., S.A. Carter, Phys. Rev. B 49 (1994) 7088.
[31] A. Labarta, R. Rodriguez, L. Balcells, J. Tejada, X. Obradors, F.J. Berry, Phys. Rev. B 44 (1991) 691.
[32] D. Fiorani, S. Viticoli, J.L. Dormann, J.L. Tholence, A.P. Murani, Phys. Rev. B 30 (1984) 2776.
[33] J. Romero-de-Paz, M.T. Fernandez-Diaz, J. Hernandez-Velasco, R. Saez-Puche, J.L. Martinez, J. Solid State Chem. 142 (1999) 29.
[34] M.T. Fernandez-Diaz, J. Rodriguez-Carvajal, J.L. Martinez, G. Fillion, F. Fernandez, R. Saez-Puche, Z. Phys. B: Condens. Matter 82 (1991) 275.
[35] D.K. Han, S.H. Kim, K.P. Hong, Y.U. Kwon, S. Kim, J.S. Lee, J. Solid State Chem. 177 (2004) 1078.
[36] K. Hong, Y.U. Kwon, D.K. Han, J.S. Lee, S.H. Kim, Chem. Mater. 11 (1999) 1921.
[37] J.E. Millburn, M.J. Rosseinsky, J. Mater. Chem. 8 (1998) 1413.
[38] E.E. McCabe, C. Greaves, Chem. Mater. 18 (2006) 5774.